SHEAR LAYER MODELS AND COMPUTER ANALYSIS OF DATA

Javier JIMENEZ
UAM-IBM Scientific Center
Castellana, 4, Madrid-1, Spain.

R. MARTINEZ-VAL and M.A.HERNAN
Universidad Politécnica, Madrid.

Introduction

Modelling a turbulent flow involves more than predicting its technologically interesting properties. While it is probably true that a better model will predict better the separation of a boundary layer, the converse is not necessarily true; quite as important is the amount of insight gained. This is difficult to define. Appart from a certain amount of esthetic appeal that makes you feel that you have "understood" a certain situation in a certain case, insight has something to do with minimum complexity and with the facility of including new features starting from a given model.

Thus, once we are able to use Prandtl's lifting-line theory to compute the behaviour of a slender wing, we can hope to understand which are the effects of body-wing interaction, even if for it we need to put the problem in a computer. However if we use a large computer simulation just to study the behaviour of the wing profile, even if the results are probably much better than those of the simple theory, chances are that the complete problem will soon be outside the bounds of available computer power or programming complexity. The lifting-line theory is a less accurate predictor but gives more insight.

A different question is how to construct good models. An useful approach is to break the big problem into smaller modules and to try to understand them one by one. The problem then is to validate the pieces. If one wants to keep the submodels understandable and simple it is often necessary to purposely neglect some effects, even if they are known to be important for the final predictions. Therefore these predictions cannot be used to check whether the model is good, and we need experimental results relating only to the partial aspect under study. This has been traditionally difficult to do, specially in turbulence where the experimental signals are complex. Instead, the usual approach has been to see what quantities can be measured and to tailor the models so that they can be validated with those quantities.

This has changed with the introduction of the digital computer as an integral part of the data reduction process. It is now possible to analyze a complex signal and isolate from it, using pattern recognition techniques, specific features relating to

a particular aspect of the flow and to use these features to validate submodels.

Two examples are given in this paper, both relating to the plane mixing layer. This flow is a good test case for modelling and experiments. Its two-dimensionality, at least in the initial region, makes it easier to understand than almost any other turbulent flow and, in addition, a large amount of experimental and theoretical work has been done on it in the last few years.

There are two different aspects of the mixing layer. First, the flow field. At the exit from the splitter plate we have the continuous creation of a thick vorticity sheet that immediately develops a wavelike instability resulting in the formation of vorticity "knots" at regular intervals. This linear phase is well understood and the theoretical predictions agree well with experiments [1, 2]. There is less agreement in the subsequent nonlinear evolution. It seems clear that the vorticity concentrations keep growing and form the seeds of the large coherent structures that are observed later. Since total vorticity is essentially conserved at large Reynolds numbers the growth of the knots, or "cores", can only happen by the amalgamation of several of them into bigger structures. Two mechanisms have been proposed for this amalgamation; historically the first observations were described as "pairings" [3], in which two vortices rotate around each other and become somehow entangled to form a single entity. If we momentarily think of the cores as point vortices this process is easy to understand. A row of vortices is unstable and the dominant mode of instability results precisely in the common rotation of pairs of contiguous vortices. The subsequent entanglement does not result from this model but, in some sense, a pair of rotating cores can be considered a bound state with twice as much vorticity.

A different process, "tearing", was proposed in [4]. Here the finite size of the cores is essential; under some circumstances the cores themselves desintegrate, their vorticity is set free and eventually the neighbouring cores absorb it and grow.

The dynamics of vorticity evolution is a complex nonlinear phenomenon which is not easy to study without the use of simplified models. We address this matter in the second example in this paper in which a particular aspect, the mechanism of amalgamation, is modelled; in fact it is neglected. The predictions, or rather the parameters to be used in the model are then studied by a computer analysis of anemometry measurement in a mixing layer.

This evolution has a parallel in the behaviour of the concentration field. This is a much simpler problem; once the velocity field has been described (or assumed) the transport of a passive scalar property is a linear process which can be computed easily. Also the experimental evidence is more complete; the beautiful films of the mixing regions, specially those by the GALCIT group, contain enough information to completely define the two-dimensional evolution of the concentration field.
In the next section we try to check some basic ideas; by just assuming that each

concentration eddy contains a region of active vorticity and that these regions evolve more or less independently of one another, and therefore obey similarity rules depending only on their own size, we deduce a series of statistical parameters on the lifetime of each eddy. The different consequences of pairing and tearing are also discussed.

The point of view in this model is essentially Lagrangian, as opposed to Eulerian, in that the evolution of each eddy is followed individually. As a consequence the predictions are also Lagrangian and have to be extracted with care from the visualization films; this we do using digital image processing. The computer is trained to recognize the eddies, draw an x-t diagram and measure such quantities as eddy areas, positions and lifespans. The results are compared with the theoretical model.

The concentration field

In modelling the homogeneous mixing layer we will always make the assumption of temporal rather than spatial growth. The velocities of the top and bottom streams will be taken to be $\pm$ 1/2, so that the vorticity in the layer is stationary in the average. Since the spreading angle of physical layers is small and since we will be neglecting in general the interaction of an eddy with all but its most immediate neighbours, this approximation is not critical. The transformation to the spatial case, when needed, will be done by the obvious Galilean transformation with a convection velocity U_c.

After the initial instability phase we assume that the vorticity is concentrated in a row of relatively compact cores. These cores act at large distances like point vortices and tend to roll one of the streams into the other, producing a spiral structure of the concentration field that grows with time [5]. This process continues as long as neighbouring structures do not interfere with each other, in effect exhausting the supply of available unmixed fluid; at this moment the structures ("eddies") will stop growing unless an amalgamation rejuvenates the situation by providing more growing space for each eddy.

For an incompresible fluid the amount of material entrained in an eddy is proportional to the eddy cross section, which can easily be measured on the visualization films. What happens to this area in an amalgamation depends on the details of the process;in a pairing the area after amalgamation will be the sum of the areas before, plus possibly a fraction entrained during the process. In a tearing an eddy will just disappear and the neighbouring ones will absorb its fluid, increasing its area proportionately.

Consider now the characteristic lengths in the flow. In the absence of viscosity and of long range interactions (splitter plate, etc.) the only length available to an eddy is its wavelength, the distance to its neighbours, and this should be equal

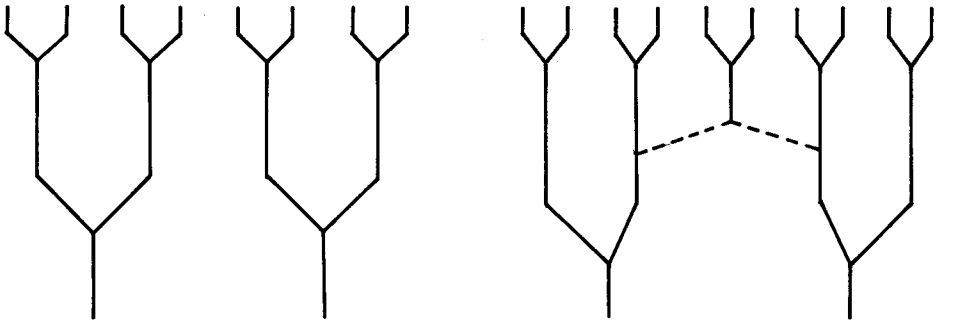

Fig. 1.- Sketch of x-t diagram for eddy motion. a: Only pairing; b: Pairing and tearing present.

in the average to the vorticity contained in the core, normalized with the velocity difference. Consider a simple case in which the only interaction is by pairing (fig. 1.a). After each pairing the vorticity in the average eddy doubles, and so do all scales; therefore the area should increase by a factor of four

$$S_{0(n+1)}/S_{0n} = 4 \qquad (1)$$

Consider a more complicated situation in which there is a certain amount of tearing (fig. 1.b), so that at the end of its lifetime each vortex has increased it vorticity by a fraction τ, received from the teared nearby eddies. By the same argument as before the area increase in one generation will be

$$S_{0(n+1)}/S_{0n} = 4(1+\tau)^2, \qquad (2)$$

and by measuring this ratio we can get an estimate for τ.

This area increase can be divided in two parts, the increase during the roll-up and that during the pairing. This separation can not be deduced from the similarity arguments proposed here but is interesting since the two opposing views have been forwarded: that growth is due to pairing [3] and to roll-up [5]. We will come back to this problem when analyzing the experiments.

There is one further prediction that does not depend on the details of the growth mechanism. After one generation the eddy scales increase by a factor of $2(1+\tau)$; the lifetime of each generation will increase accordingly and for an eddy born after the n-th pairing the lifetime will be

$$T_n = 2^n(1+\tau)^n T_0.$$

Going back to the spatial case, during this time the eddy has moved a distance $U_c T_n$,

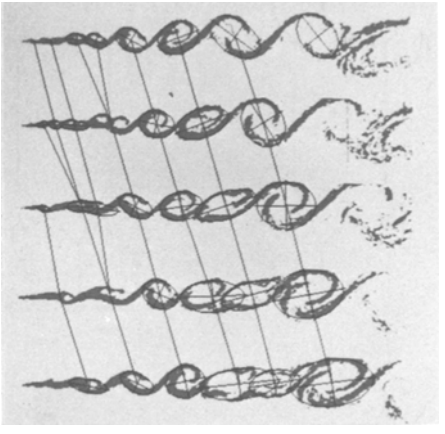

Fig. 2.- The x-t diagram for five frames as interpreted by the computer analysis program.

so that the distance from the n-th pairing to the splitter plate is

$$X_{0n}=U_c \sum_{k=1}^{n-1} T_K=U_c T_0(2^n(1+\tau)^n-1)/(1+2\tau)$$

and the normalized lifetime after a few amalgamations is

$$\frac{U_c T_n}{x_{0n}} = 1+2\tau, \qquad (3)$$

which can also be used to estimate τ.

Both the lifetime and the evolution of eddy cross section can be measured directly from the visualization films. Doing this by hand, however, presents several problems, arising basically from the large number of frames to be processed; there is the shear amount of repetitive work involved in measuring several thousand objects in a consistent manner, and the need to keep a unifom criterium all this time in such subjective matters as the exact boundaries of an eddie or the moment of amalgamation. This is why we decided to let a computer do the measurement. The actual processing is described elsewhere [6,7] but the relevant results and the outline of the method are given here.

A continuous sequence of frames (~400) from a film of a homogeneous mixing layer, kindly provided to us by Prof. Roshko, is digitized in a scanner reducing them to numerical matrices in which each element is proportional to the optical density of the film in the neighbourhood of a given point. This two-dimensional digital signal is then enhanced, filtered and simplified until each frame is classified into zones of mixed and unmixed fluids. The outline of these zones is extracted and the computer is given a series of rules by which it can segment the outlines into individual eddies, to each of which it fits an ellipse which is taken to represent the eddy shape and position. It is now an easy task to follow the motion of these ellipses accross different frames and to organize them into coherent histories.

Each history begins either with the appearance of a new eddy that can not be assigned an ancestor in a preceding frame, or as the merging of two (or several) previous histories. Similarly, histories end either when there is no reasonable continuation in a subsequent frame, or when they merge with a neighbour in an amalgamation (see fig. 2). The process by which a history suddely disappears to merge with appreciable probability with two different neighbours was not forbidden in principle, but was found only seldom (20 times is nearly 700 histories). When

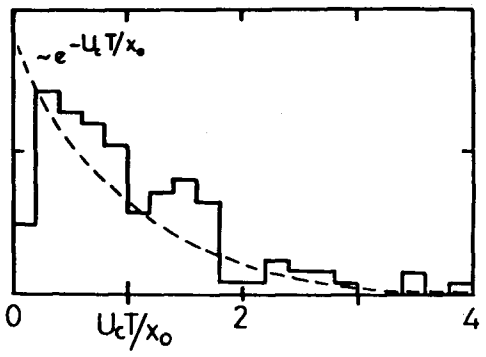

Fig. 3.- Histogram for nondimensional lifetime of eddies. Aver: 1.05 ± .77, Sample: 114 histories.

those cases where inspected visually, they were seen to correspond in all cases, but one, to small errors in the recognition procedure and to have in any case a clearer interpretation as pairings to one of the neighbours. The remaining case is our only documented candidate for a fast tearing.

The lifespan statistics are given in figure 3, in which only those histories starting and ending with amalgamations have been considered, and which should therefore correspond to equation (3). The average normalized lifetime is 1.05, implying a tearing frequency very close to zero; also the histogram is approximated reasonably well by an exponential distribution with parameter equal to one, confirming the value of the average. A similar histogram was presented in [8] but, even if the distribution was also exponential, the average was lower (.45) and therefore inconsistent with equation (3).

Figures 4(a-b) give histograms of area increase during roll-up and pairing. Again only histories beginning and ending with pairings have been considered, and equation (2) should hold. A slight correction might be needed since some of the interactions involve more than two eddies, but the effect is small and is not taken into account.

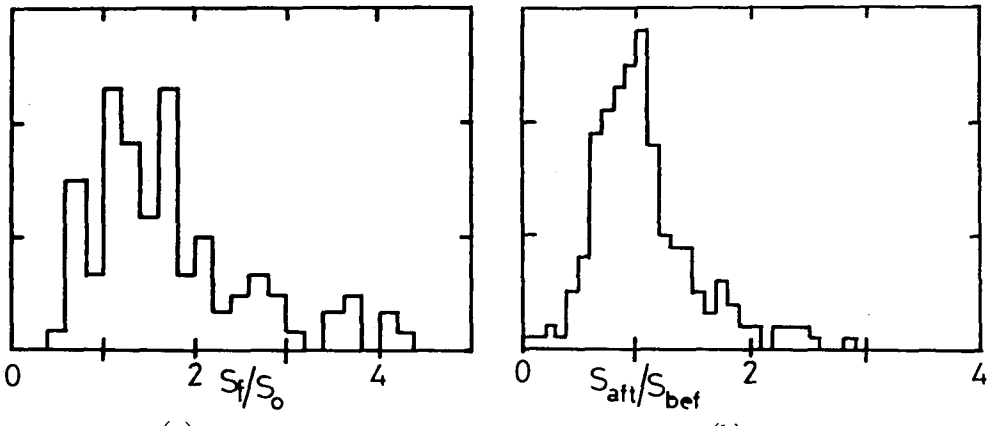

(a) (b)

Fig. 4.- Histograms for eddy area growth. a: Area ratio from beginning to end of lifespan; Aver.: 1.75 ± .87, Sample: 91 histories. b: Ratio of total area before and after amalgamation; Aver.: 1.17 ± .45, Sample: 210 amalg.

Actually, out of 210 amalgamations studied, 196 are pairings, 14 triplings, and none is a quadrupling. It is interesting that in the average most of the area increase happens during the roll-up (1.75) and relatively little fluid is entrained in the pairing (1.17), in accordance with the idea that the entraining is due mainly to the active vorticity in the eddy cores. The average eddy increase in a generation is obtained by multiplying the average increase ratios in these two processes, times the number of vortices involved in a pairing, so that

$$S_{0(n+1)}/S_{0n} = 2 \times 1.75 \times 1.17 = 4.1,$$

which, compared with equation (2) implies again that essentially no tearing is present.

A more direct counting of pairing versus tearing is possible. Choosing the center part of the layer to avoid complications due to end effects, we counted directly the number of histories beginning and ending in different ways. In this region 96 histories began as a consequence of pairing while 20 started out of nowhere. These last ones were considered recognition errors, an interpretation confirmed by visual inspection. On the 145 histories ending in a pairing, a similar error rate would give 31 mistakes, while the actual number of histories ending without descendency was 36. The excess of 5 histories (out of 181) is a new estimate of the frequency of tearing. Actually, after displaying several cases in which histories ended without pairing, we found that, appart from obvious mistakes, there is a process accounting for these eddy disappearances.

In it, an eddy, usually small with respect to its neighbours, stops growing and is slowly stretched, or bleeded, by them. The process usually takes several frames and is different from the more or less rapid desintegration of an eddy of which we mentioned a single example above. Its frequency is consistent with the estimate of a few percent that is implied by the measurements of area growth and lifespan.

Thus, in all, the results of the computer analysis of the visualization films confirm the idea that eddies grow mainly by roll-up, and almalgamate by pairing. Tearing is observed, but it appears to be a relatively rare event of little importance in the global dynamics of the layer.

Modelling the vorticity field

The results presented above show that from the point of view of the concentration interface the plane mixing layer can be modelled by a more or less one-dimensional row of vorticity blobs, one within each of the concentration eddies.

Unfortunately this does not tell us much about the internal structure of the blobs. In fact, any concentration of vorticity whose effective diameter is less than the size of the concentration eddies will generate around itself a closed streamline

and behave from the outside much like a point vortex. Besides, pairing is a major difficulty; in the above discussion it was assumed that when instability of the row brings two cores near one another they somehow merge into a single one.

Two isolated point vortices will not merge but move around each other in a permanent orbit. Tearing, on the other hand, is explained because cores of finite size, when subject to too much strain, become unstable and desintegrate. As cores move downstream in the layer, they grow in size until the strain produced by the collective effect of the vortex row is enough to destroy them [4] . However, the instability mechanisms involved in pairing and tearing are basically the same and the time scales involved are at most similar, while for compact cores pairing is always more unstable. Therefore we would expect to find in a mixing layer mostly pairing interactions with an occasional tearing, as is indeed the case in the experiment reported in the last section.

This still does not explain the merging of the cores involved in a pairing. One possibility, is that the strain induced by the close approach is again able to destroy the cores, which then reform together. However it can be shown [5] that the maximum strain in a vortex row occurs when the cores are at their undisturbed position and that the strain actually decreases when they come together in a pairing; therefore if the cores do not desintegrate before they begin to pair they will not do so afterwards.

Another possibility is viscosity, but the effect will be dependent on Reynolds number and will imply that for low viscosity the cores may orbit for long times without merging, even after the concentration eddies have coallesced completely. Numerical simulations of the mixing layer usually include some viscosity, although seldom in a well controlled way. In some cases [9,10] merging of the vorticity structures is very apparent in the results, while in others [11,12] vortex cores are seen rotating around each other for a long time without merging. Because of the different integration schemes used it is difficult to say whether the effect is real or a computational artifact.

A curious fact is that the easiest and probably one of the most succesfull numerical modellings of the mixing layer actually involves no pairing at all. A large number of point vortices, with some kind of short-range cutoff,are used to simulate an initial vortex sheet which is perturbed slightly, and the motion of the points are used to follow the subsequent behaviour of the layer [10,13,14]. The cutoff seems to be important to avoid numerical difficulties, but the details of how it is done do not seem to affect strongly the outcome.

The results of one such simulation are shown in figures 5 and 6. A hundred point vortices are distributed uniformly along a segment on the x axis and their initial positions are perturbed slightly before starting the integration. The whole

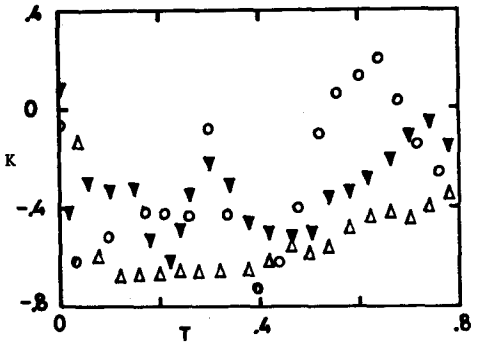

Fig. 5.- Evolution of kurtosis of lateral distribution of vortices in simulation. $K=\mu_4/\sigma^4-3$.

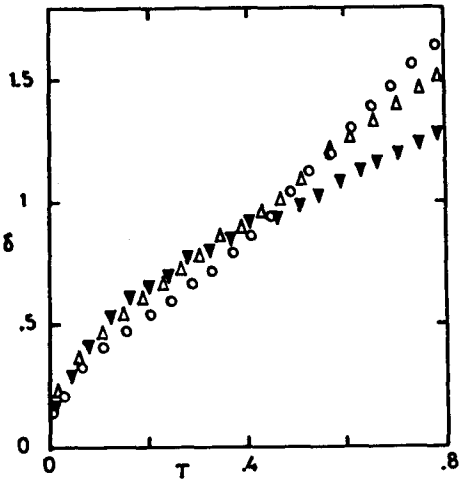

Fig. 6.- Vorticity thickness growth in point vortex simulation. Different symbols are different simulation parameters.

arrangement is assumed to be periodic in x and the short range cutoff is provided by using a look-up table to compute the induced velocities (for a similar method see [15]). Each of the curves in the figures is an average over five independent random initial conditions.

As soon as the integration begins, the vortices start to scatter laterally. Since all vortices have the same strength the probability density of this distribution is proportional to the average vorticity profile accross the layer and the average velocity can be obtained by simple integration.

Because of the symmetry of the equations of motions, if the odd central moments of this distribution are initially zero, they remain so forever and the distribution is determined by its even moments. The evolution of kurtosis is shown in figure 5; even if it shows wide oscillations it seems to drop very fast to about -.5 and to stay around that value. That implies that the vorticity profile is almost gaussian, but slightly flatter, in agreement with experimental measurements. Disregarding the deviation from gaussianity the velocity profile will be an error function and the vorticity thickness $(\partial u/\partial y)^{-1}$ will be proportional to the standard deviation

$$\delta = \sqrt{2\pi}\,\sigma \,. \qquad (4)$$

This is represented in figure 6 for three different combinations of numerical parameters and it is seen to grow linearly in all cases, with growth rates (.11-.18) that again agree well with experimental evidence.

Since at least the mean velocity profile of the mixing layer is described so well by

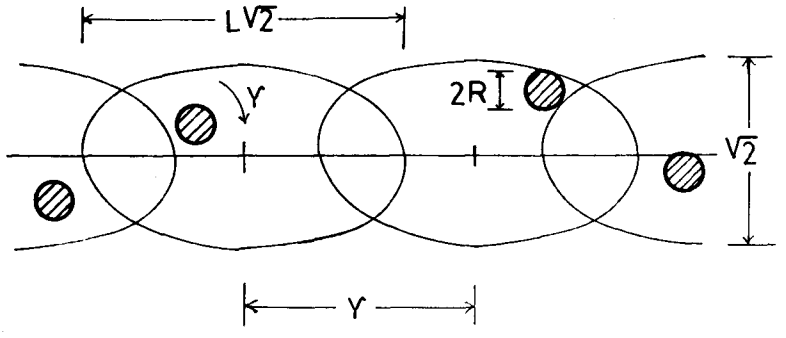

Fig. 7.- Geometry and scatter ellipses for the vortex cloud model.

a model that neglects such pressumably basic features as vortex core sizes, amalgamations and large scale structure, it is interesting to explore how far can other average properties be computed from a simple description of the layer as a cloud of vortices with the correct lateral scatter.

Consider an arrangement consisting of a row of solid vortex cores with strenght γ and radius R distributed more or less uniformly along the X axis. If the units are taken so that the velocity jump is one, the average longitudinal distance among vortices is also γ. The position of the n-th core is a random variable distributed normally around the center point $(n\gamma,0)$ with variances which are 1/2 in the transverse (y) direction and $L^2/2$ in the longitudinal one, so that the density function is

$$P_n(x,y) = p(x-n\gamma,y) = \exp\ (-y^2-(x-n\gamma)^2/L^2).$$

To simplify calculations the positions of all vortices are assumed to be mutually independent, and the spirit of the model will be to think of R and γ as small numbers (see fig. 7). Somewhat surprinsingly the resulting velocity distributions are found to depend not only on R and γ but on the longitudinal scatter L, and, while vortex size and strength are measurable physical properties, the scatter is a parameter of the model that has to be computed theoretically.

Happily the total energy associated with the vortex distribution is also a function of L and can be used to decide which value to use. For point vortices the excess energy (per vortex) with respect to the uniform row is proportional to [16]

$$E = -\int_{-\infty}^{\infty}\int\int\int\int \sum_{n\neq 0} \log \frac{(x-x')^2+(y-y')^2}{n^2\gamma^2} P_0(x,y)P_n(x'y')dx\ dy\ dx'\ dy', \qquad (5)$$

which can be manipulated into the form

$$E = -2\pi^{-3}\gamma^2 L \int_0^{\infty}\int \log \frac{\sin^2\xi+\mathrm{sh}^2\eta}{\xi^2+\eta^2} \exp \frac{-\gamma^2(\xi^2/L^2+\eta^2)}{2\pi^2}\, d\xi\ d\eta, \qquad (6)$$

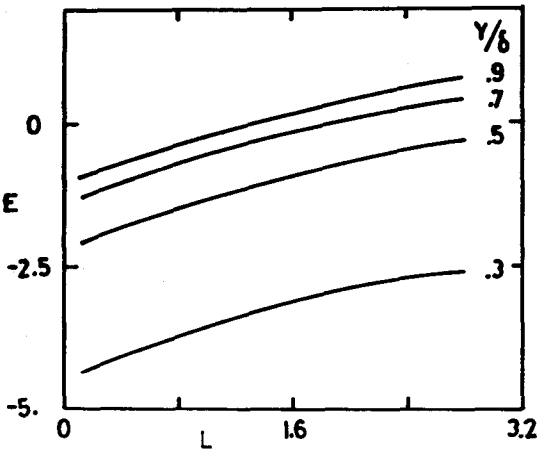

Fig. 8.- Excess cloud energy due to vortex scatter.

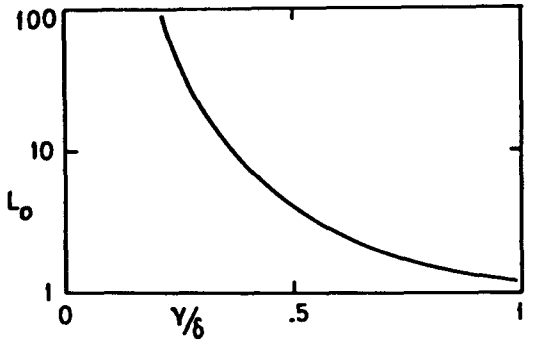

Fig. 9.- Longitudinal vortex scatter for zero energy, as a function vortex strength.

and then evaluated numerically. The effect of R on this energy is slight and has not been taken into account. The results are given in figure 8; the energy is a monotonically increasing function of L which can be shown to increase without limit for $L\to\infty$, and the minimum energy occurs for L=0. Intuitively, as the scatter of the cores gets bigger, the probability of two vortices getting very close to one another gets higher and this makes the average energy larger. We can then expect that the most probable configuration is that with the minimum energy and that we should use L=0 in our model.

Another possibility is to use the value of L that makes the excess energy equal to zero, as in a purely inviscid calculation in which the initial condition is very close to an uniform row, we expect to end up in such a state. The values of L satisfying that condition are given in figure 9 and all calculations in this section are presented for the two cases: zero and minimum energy. However it should be remembered that the natural evolution of a vortex row will not produce in general uncorrelated vortex positions and that it may not be consistent to force energy conservation at the same time as neglecting the correlations.

The average velocity profile is independent of L and γ and to the lowest order in R is an error function. The finite size of the cores has the effect of thickening slightly the layer so that the vorticity thickness is given by

$$\delta \simeq \pi^{1/2} (1+R^2/4) + O(R^4). \qquad (7)$$

The turbulent intensities depend critically on the core radius. For point vortices the integral of the square of the velocity diverges when the integration path

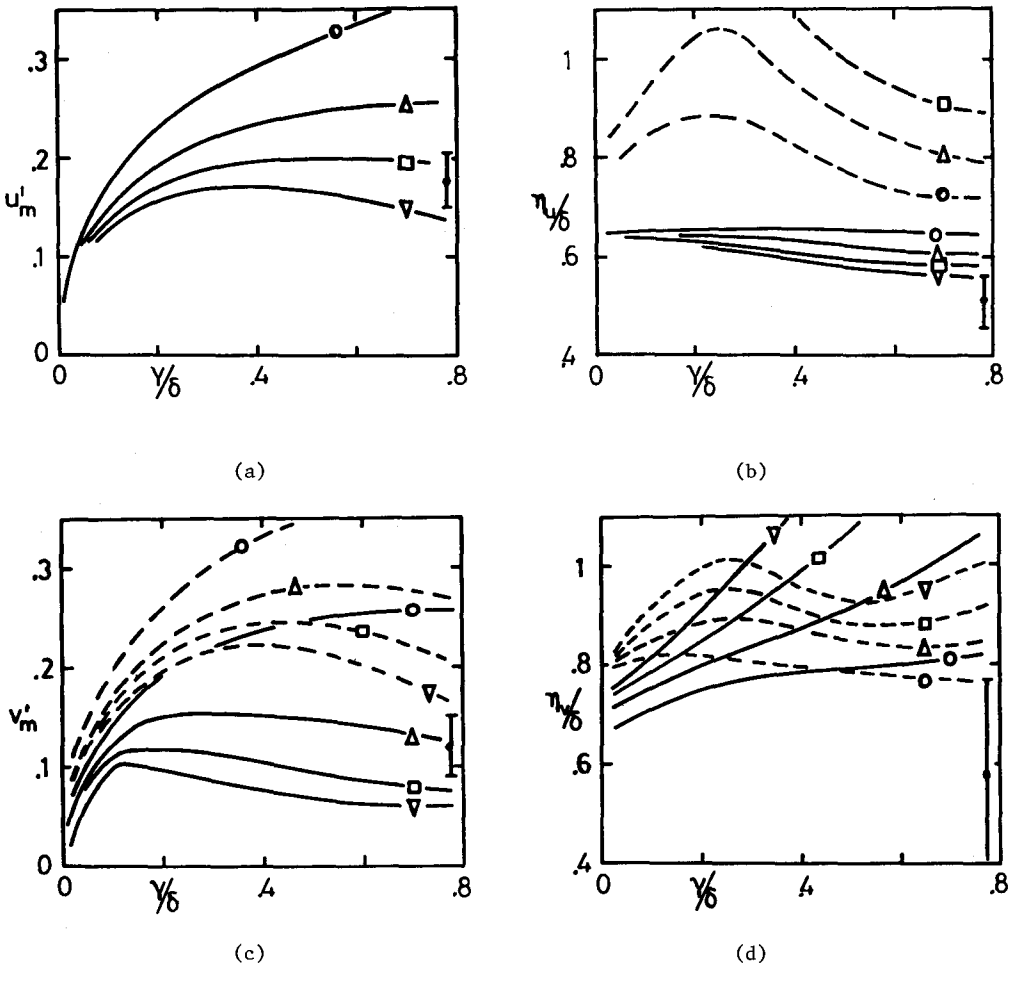

Fig. 10.- Results of vortex cloud model. O: R/γ=.1, Δ:.3, B:.5, ∇:.7; Continuous line is for minimum energy (L=0), dashed is for zero energy. a.- longitudinal turbulence level; b.- u' profile half-width; c.- transversal turbulence level; d.- v' profile half-width.

crosses a core, and all intensities are infinite. Consider the longitudinal fluctuations for finite cores. The velocity induced by a vortex is

$$u(x,y) = \begin{cases} \frac{\gamma}{2\pi} \frac{y}{x^2+y^2} ; & x^2+y^2 \geq R^2 \\ \frac{\gamma}{2\pi} \frac{y}{R^2} ; & x^2+y^2 \leq R^2, \end{cases}$$

and the variance produced on (x,y) by a single vortex is

$$\sigma^2(x-n\gamma,y)= \iint_{-\infty}^{\infty} u^2(x-\xi,y-\eta)p(\xi-n\gamma,\eta)d\xi\ d\eta -[\iint_{-\infty}^{\infty}u(x-\xi,y-\eta)p(\xi-n\gamma,\eta)d\xi\ d\eta]^2 \quad (8)$$

Since the positions of the vortices are uncorrelated, the variances are additive and the fluctuation level is found by adding the individual variances and averaging the result over x,

$$u'^2(y) \approx \frac{1}{\gamma}\int_0^{\gamma}\sum_n \sigma^2(x-n\gamma,y)dx = \frac{1}{\gamma}\sum_n\int_{-n\gamma}^{(-n+1)\gamma}\sigma^2(x,y)dy = \frac{1}{\gamma}\int_{-\infty}^{\infty}\sigma^2(x,y)dy, \quad (9)$$

which can now be expanded in R and evaluated numerically. The results are given in figure 10.

Figures 10 a,c give the maximum (y=0) longitudinal and transversal fluctuation intensities (note that u' is independent of L). The other two graphs characterize the shape of the fluctuation profiles by giving the value of y for which the fluctuation is half of the maximum. In all four cases there is a vertical error bar in the right hand side of the plot showing a representative range of the experimental values for the quantities involved, collected from the available literature [17-21].

Any model with two adjustable parameters is bound to predict something and no judgement can be made until R and γ are measured directly from a mixing layer; this is done in the next section. However several conclusions can be deduced from figure 10. First, in all cases de minimum energy assumption (L=0) works better than the zero energy one. Next the peak intensities, both u' and v', are reasonably well predicted by $R/\gamma\sim.3-.5$ and a wide range of γ; this is in good agreement with the results in the next section. Finally the half width for both profiles are overestimated by about 30% but still within the right order of magnitude.

An important failure of the model is in the prediction of the Reynolds stresses. The prediction is zero, and this is a fundamental consequence of the parity of the velocity components of a vortex and of the hypothesis of zero correlation. No stresses obviously mean no layer growth and no momentum diffusion. In the numerical experiments, in which the rate of growth is accurately represented, there is a large scale clumping that introduces a correlation of vortex positions and looks strikingly like the coherent structures in real layer. In this sense it seems that the large structure is responsible for the dynamics of the mixing layer even if most of the commonly measured quantities u, u' and v' are predicted well by a purely kinematic description in terms of small vortices randomly distributed.

Measuring the core parameters

In the last section we have found another case in which, to check a given model, we need some elaborate processing of the experimental data to extract the required information. The properties to be measured are now the radius and circulation

associated with the vorticity cores in the mixing layer and the appropriate signal is a hot wire velocity reading.

Some similar studies have been reported before. Browand and Weidman [22] and several other authors have mapped the vorticity distribution in the large structures by phase averaging and find single peaks in the center of the structure. However, averaging is intended precisely to smooth the differences in the internal arrangement of the different eddies and will give at most the probability distribution of the position of the small vortices, if they exist. Another attempt was done in [23] where individual eddies are studied, with no averaging, but the probes are positioned far outside the mixing layer and the effect of the small vortices is integrated by the distance.

To be able to see vortices which are small with respect to the large structure we need to observe them from distances which are smaller than the vorticity thickness. Think of a vortex passing so near our probe that locally its influence dominates the flow, but still far enough that we stay outside the rotational core; we will see something similar to the velocity induced by a point vortex and, from this velocity, we should be able to deduce the properties, circulation and distance, of the passing core.

Unfortunately, in most cases the situation is more complicated; either there are several cores at roughly the same distance from our probe, so that our signal is complex and difficult to analyze (figure 11-a), or else the path of the cores intersect the probe and the signal is strong but does not follow the behaviour of a simple point vortex (fig. 11-c). Occasionally however a core will just skirt the probe at just the right distance, and produce a clean peak that can be detected and analyzed (fig. 11-b).

We have used these peaks to study the vortex cores in the shear layer. We used a plane continuous air half jet discharging in a large room. The stream velocity was 50 m/s with a turbulence level of .3%, and the nozzle section was 130x70 mm. The boundary layer at the splitter plate was laminar, although close to transition, and its peak turbulence level reached 1-2%. The apparatus is described in detail in [24]

A hot wire anemometer was used to take longitudinal velocity and turbulence profiles at several sections and, in addition, long records (20 s) were obtained at several point for use in the peak recognition studies. Two examples of the signal are given in figure 12. The first record corresponds to the region of linear instability in which compact cores have pressumably not yet formed. The second is further downstream, after one or two large scale amalgamations, and is more complex. Large peaks appear in it that seem to have roughly the same scale as the ones in the linear record, but they happen less often and, in fact, it looks as if every second peak is missing, suggesting that the effect of the amalgamation has been not to produce bigger cores but to displace half of them out of sight from our probe.

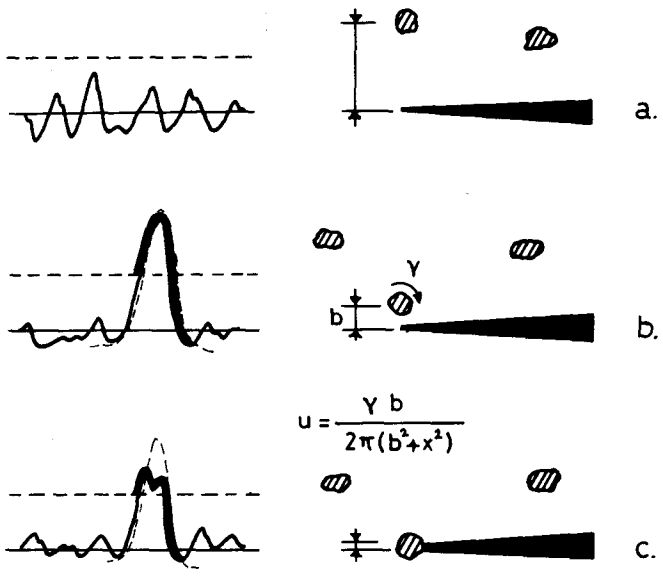

Fig. 11.- Relation between different relative positions of passing cores and signals detected by probe.

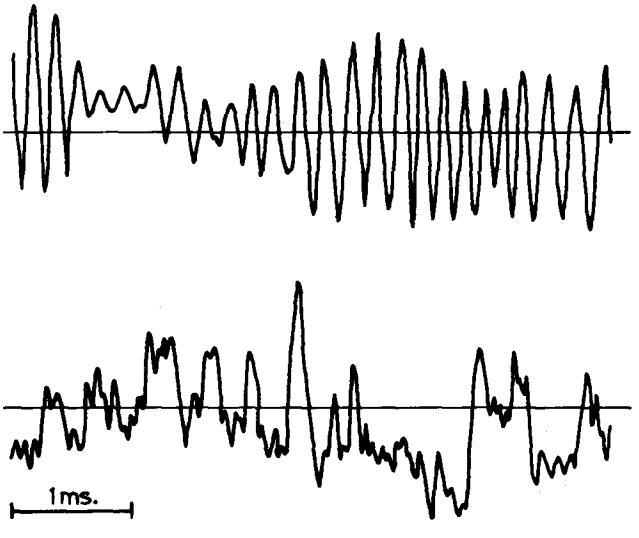

Fig. 12.- Examples of signals used in the peak recognition procedure. Top record is in the linear transition region (x=10 mm), bottom record after one amalgamation step (x=30).

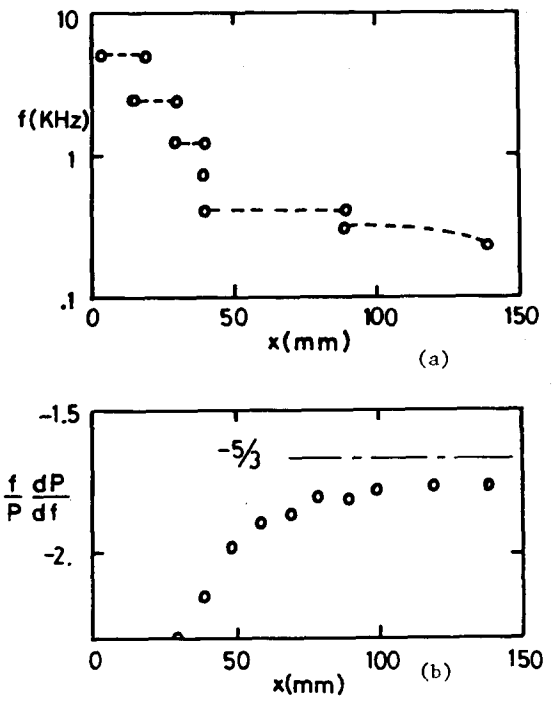

Fig. 13.- Spectral evolution of mixing layer vs downstream coordinate. a: Frequency of dominant spectral peak; b: Slope of inertial power spectrum range.

The development of the layer, as seen from th power spectrum of the velocity fluctuations, is documented in figure 13. In 13-a the frequencies of the dominant spectral peaks are given as function of downstream coordinate. They show periodic halvings that should correspond to the average position of the large scale amalgamation events. Figure 13-b shows the evolution of the slope of the inertial range in the (log-log) spectrum. Pressumably the moment where this slope attains the Kolmogorov value of -5/3 marks the beginning of full flow three-dimensionality and well developed turbulence. The records on figure 12, as well as all the results to be presented below are taken in the region in which the three-dimensional regime has not yet been entered.

The details of the peak recognition process are given elsewhere [25]. Essentially a long record is obtained, stored in digital tape, transformed to velocity and thresholded to identify the very large peaks. The thresholder detects every instance in which the velocity exceeds a certain value and then falls again below a different, lower, one.

Once a peak is found it is isolated from the record; its end point is the first minimum after crossing the downgoing threshold, and is taken to define the level of the "base" velocity, i.e. the velocity which would be observed if the core under consideration were removed from the layer. After substracting this level, the peak should be approximated by the velocity induced by a point vortex (figure 11-b).

$$u = \frac{\gamma/2\pi b}{1+(U_c t/b)^2}\ , \qquad (10)$$

where U_c is the unknown convection velocity of the vortex core. This equation is fitted to the shape of the peak and only those instances that show a reasonably good fit are accepted as real cores, thus rejecting all but the clear-cut cases. The acceptable error and the different thresholds are adjusted empirically so as to

make the final results as independent of them as possible.

By this procedure we can get values of b/γ and U_c/b but, to get absolute circulations, we need to make hypothesis on U_c. We have used the assumption that the cores move with the average flow velocity at their transversal co-ordinate which, linearizing around the probe position, is

$$U_c = U_p + (\partial U_p/\partial y)b, \qquad (11)$$

where U_p is the average velocity measured by the probe. This hypothesis permits us to compute values of γ and b for individual cores and to compile statistics for them.

Its accuracy is only approximate; inspection of the velocity records obtained at different transverse probe positions shows that the peaks are indeed wider at the low speed side of the layer, indicating that they are convected slower, and the ratio of the widths corresponds roughly to the ratio of the average velocities. A more quantitative estimate of the influence of the hypothesis in the accuracy of the final results can be had from figure 14. There we can see the values of the average vortex circulation obtained at three different sections, with the probe at different transverse positions. Since there is no "a priori" reason why cores should look different when seen from different points of view, the drift apparent in the figure is probably a measure of the inadecuacy of assumption (11) and a measure of the final errors to be expected.

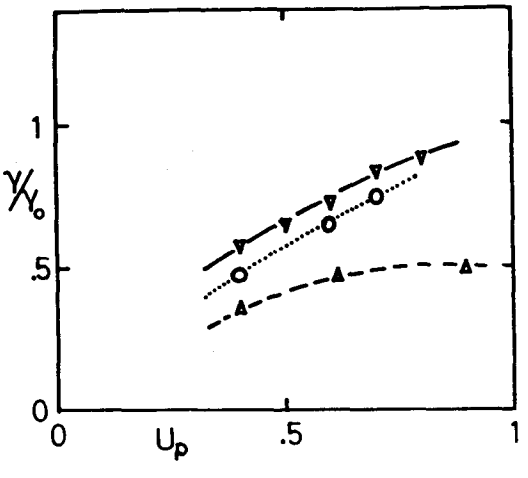

Fig. 14.-. Cross-stream variation of measured average circulation per core vs. velocity at probe position.
Δ: x=20 mm, 0: 40 mm, ∇:60 mm.

These errors have another consequence: equation (11) has a different effect on the accuracy of γ depending on whether the core is positive ($b<0$) or negative. Analysis shows that the resulting errors tend to cancel for positive peaks, so that the results are quite accurate in this case, while for negative peaks they reinforce each other, giving unacceptable results. Only positive peaks will be used below.

In summary, by observing the strong peaks in the velocity records, and subject to assumption (11), we are able to measure the strength and distance of the passing cores. The parameter b/γ is independent of (11)

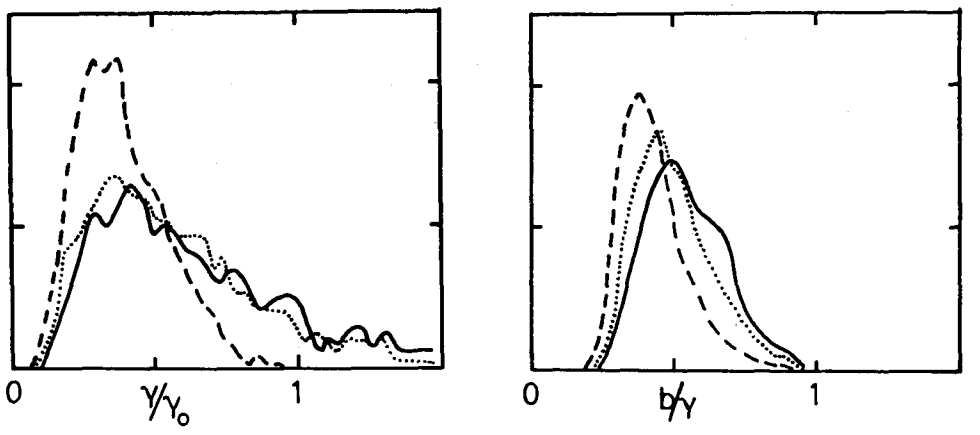

(a) (b)

Fig. 15.- Histograms for core strength (a) and normalized distance to probe (b). ---:x=20 mm, ...:40 mm, -: 60 mm.

and the measurements should be accurate, while the absolute circulation and distance show large errors and should be taken only as indicative values.

The final histograms at three different downstream stations are given in figure 15. The vortex strength is shown normalized with the circulation γ_0 corresponding to the wavelength of the initial instability of the shear layer. It is rather surprising that in all cases the most probable value is smaller than one, and is actually close to .5. It is noteworthy in this respect that the structure of the most unstable mode predicted by the linear stability theory consists precisely of two vorticity concentrations, one "on top" and the other on the "bottom" of the initial perturbation, each containing half the vorticity of one wavelength, and rotating around each other in a pairing motion (fig. 10 in [2]). Even if it is not clear whether this solution continues to be valid after the initial moments, it is tempting to speculate that the cores observed in fig. 15 are those initial vorticity concentrations, many of which have not disappear by merging even at the most downstream station. Actually the circulation distributions at the second (x=40) and third (x=60) stations are almost identical, even if by then the large scale structures have suffered at least two and four amalgamations steps.

The distance data is easier to understand. At each station the histogram shows that no cores are detected either very near or very far from the probe. This was expected since vortices passing too far are simply lost in the general background while those passing too near intersect the probe and are rejected by the fitting algorithm. In fact the lower edge of the histograms can be used to estimate the radius of the cores. From figure 15 this radius increases slightly downstream but is always in the range $R/\gamma \sim .3.-4$. This corresponds nicely to some simple theoretical modelling; if we assume that the initial vortex sheet roll-up happens without strong

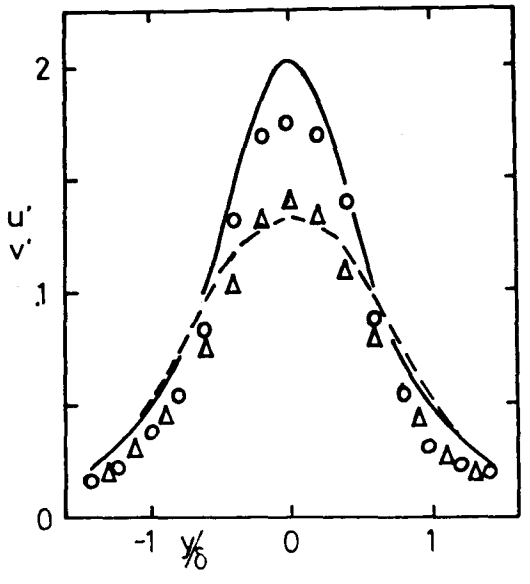

Fig. 16.- Comparison between uncorrelated vortex model (lines) and experimental data (symbols). In model, $R/\gamma=.4$, $\gamma/\delta=.3$, L=0. Experiments are from 20 .— and 0: u'; --- and Δ: v'.

interaction among different wavelengths the moment of inertia of the vorticity distribution is conserved and the final radius must satisfy the constrain

$$48\ \pi \int_0^R \hat{\omega}(r)\ r^3\ dr = \gamma^3.$$

The value of R implied by this equation depends on the particular distribution $\omega(r)$ chosen for the vorticity in the core, but in most cases falls in the range $R/\gamma \sim .3 \div .5$, which agrees well with the experimental data.

Finally it is interesting to know which fraction of the passing vorticity is detected by the algorithm. This is easy to find since the total vorticity is known from the velocity profile and can be compared with that contained in the detected cores. The result varies at different stations but is usually in the range of 5-11%, which is actually high considering the complexity of the signals treated.

The purpose of the experiment was to try to validate the model according to which the mixing layer can be represented by a cloud of small vortex cores with a high lateral scatter. We are now in the position to introduce the values obtained here in the model developed in the last section, and check the prediction.

The average core strength can be found from figure 15 and increases only slowly downstream. Therefore the parameter γ/δ decreases, beginning at .7 for x=20 and varying between .4 and .3 in the downstream stations. It pressumably keeps decreasing slowly, although eventually the three-dimensionality might alter the picture completely.

At the last station (x=60) we get $\lambda/\delta=.3$ and $R/\gamma=.4$. Figure 16 shows the tubulence profiles both as predicted from the model using these parameters and taken from the experimental data in a different mixing layer [20]; even if part of the agreement is probably accidental, considering all the approximations involved, the general fit is surprisingly good.

Conclusions

We have shown first of all that pattern recognition methods, applied to classical signals from turbulent flows, can give information on aspects well beyond the standard statistical properties. Moreover the kind of results obtained can be changed by adjusting the processing techniques instead of the experimental situations. In this respect it is important to realize that the film used in the first part of this paper was not taken with the idea of digital image processing in mind, although it was obviously well fitted for that application, and that the anemometry results were obtained in a standard apparatus in a standard way and, in fact, were the very same records previously taken to study the spectral evolution of the mixing layer.

This intensive analysis of the experimental signals is a new application of the computer to experimental science that goes beyond the introduction of digital instrumentation and control that has been such an important feature on research laboratories in recent years. We believe this sort of analysis will become more widespread and important in the future.

Secondly, the results regarding the structure of the mixing layer are also interesting. The driving force behind the evolution of the concentration field can be described well by a series of vorticity blobs, convected with the average velocity and amalgamating periodically. The amalgamation mechanism seems to be the pairing motion of two eddies, after which the two concentration features merge into a single one; there is little fluid entrainment in this phase.

It also appears that the structure of these vorticity blobs is not simple and that they contain several individual vortex cores moving on bound orbits inside a common "bag". If this is true the merging of two blobs is relatively easy to understand since, instead of the desintegration and merging of two cores, all that we have to do is to tangle together two sets of already loose orbits.

The experiments in which this "vortex bag" idea is based were done in the region in which the mixing layer is still quite two-dimensional. Three-dimensionality can be expected to change the picture, since it is difficult to think of two highly kinked vortex lines coming together without wrapping around each other and essentially merging.

The size of the vortex cores used in this model and detected in the experiments correspond to what is usually identified in the power spectrum as the inertial subrange. In some sense, therefore, the random motion of these small cores is what is usually identified as turbulence and it should be interesting to see how far the study of turbulence can be taken in terms of this idea. We have shown that some properties, notably the turbulent intensities, can be modelled correctly disregarding completely the large scale order ordering of the cores, while others, such as

the Reynolds stresses, need the explicit introduction of correlations. We suggest that this type of analysis might be useful in isolating which processes are important for different aspects of the flow.

The research of one of the authors (Martinez-Val) was supported in part by the Spanish Comisión Asesora de Investigación

REFERENCES

1. Freymuth, P., 1966, J.Fluid Mech., 25, p. 683-704.
2. Michalke, A., 1964, J.Fluid Mech., 19, p. 543-556.
3. Winant, C.D. & Browand, F.K., 1974, J.Fluid Mech., 63, p. 237-255.
4. Moore, D.W. & Saffman, P.G., 1975, J.Fluid Mech., 69, p. 465-473.
5. Jimenez, J., 1980, J.Fluid Mech., 96, p. 447-460.
6. Hernan, M.A. & Jimenez, J., 1979, Turb. Shear Flows, London, p. 7.7.-7.13.
7. Hernan, M.A. & Jimenez, J., 1980, 8th World Comp. Congress, IFIP, Melbourne.
8. Roshko, A., 1976, AIAA Paper 76-78.
9. Corcos, G.M., 1979, University of California, Berkeley, Report FM-79-2.
10. Acton, E., 1976, J.Fluid Mech., 76, p.561-592.
11. Riley, J.J. & Metcalfe, R.W., 1980 AIAA Paper 80-0274.
12. Aref, H. & Siggia, E.D., 1980, J.Fluid Mech.(to be published).
13. Ashurt, W.T., 1977, SANDIA Lab Report SAND77-8613.
14. Jimenez, J., 1977,Lecture Notes in Physics, 75, p. 147-161.
15. Delcourt, B. & Brown, G.L., 1979, Turbulent Shear Flows, London, p. 14.35-14.40
16. Batchelor, G.K., 1967, An Introduction to Fluid Mechanics, Cambridge, p. 530.
17. Liepmann, H.W. & Laufer, J., 1947, NACA TN-1257.
18. Spencer, B.W. & Jones,B.G., 1971, AIAA Paper 71-613.
19. Wygnansky, I. & Fiedler, H., 1970, J.Fluid Mech., 41, p. 327-362.
20. Pui, N.K. & Gartshore, I.S., 1979, J.Fluid Mech., 91, p. 111-130.
21. Hussain, A.K.M.F. & Zedan, M.F., 1978, Phys. Fluids, 21, p. 1100-1112
22. Browand, F.K. & Weidman, P.D., 1976, J.Fluid Mech., 76, p. 127-144.
23. Koochesfahani, M.M., Catherasoo, C.J., Dimotakis, P.E., Gharib, M. & Land, D.B., 1979, AIAA J., 17, p. 1347-1351.
24. Jimenez, J., Martinez-Val, R. & Rebollo, M., 1979, Final Report USAERO 79-G-079
25. Martinez-Val, R., 1980, Ph.D. Thesis, Madrid (in Spanish).